EUROPEAN ORGANIZATION FOR NUCLEAR RESEARCH

7 October 2013

Status and plans for 2014, CERN NA63

K.K. Andersen, R.E. Mikkelsen, U.I. Uggerhøj, T.N. Wistisen[1)]
Department of Physics and Astronomy, Aarhus University, Denmark

NA63

Abstract

We summarize the status and plans for the future for the CERN NA63 collaboration.
A systematic study of the structured target 'resonance' appearing from radiation emission by electrons passing two amorphous foils positioned with separations in the range 10 – 20000 μm was performed in September 2012. The results - recently submitted for publication - confirm a previously obtained result [1] that by this method, the formation length - of macroscopic dimensions up to 0.5 mm - for the generation of MeV-GeV radiation from multi-hundred GeV electrons can be *directly* measured. In fact the results obtained allow a distinction between competing theories [2, 3], showing that it is unlikely that the correction-term introduced by Blankenbecler holds true [4].
Furthermore, with a substantially improved setup compared to the run in 2010 (where the deconvolution of synchrotron radiation prevented results in the most interesting regime below 0.5 GeV), we investigated again the impact of the Landau-Pomeranchuk-Migdal (LPM) effect with 178 GeV electrons, in particular for low-Z targets where a discrepancy between experiment and theory might turn up. Measurements with 20 GeV electrons in a Cu target shows no indication of the 'kink-like' structure seen in Migdal's theory (the most widely used) for photon energies around 300 MeV. The absence of this structure is in agreement with simulations, and is due to the 'smearing' of the effect from multi-photon emission. These results have been accepted for publication.
A short test measurement of the efficiency of production for positrons originating from electrons impinging on an axially aligned diamond crystal was also performed, where the aim in the run proposed for 2014 is to measure the production angles and energies by means of so-called MIMOSA detectors arranged in a magnetic spectrometer configuration with a permanent-magnet-based magnetic dipole. For the 2012 run, however, the track-reconstruction algorithm yields too few events, most likely due to a too low efficiency of each detector. This was not realised at the time of the test, that nevertheless was useful in establishing the functionality of the rest of the setup as well as the alignment of the diamond $\langle 100 \rangle$ crystal.

For the future, we propose to measure the production angles and energies of positrons produced by 10-50 GeV electrons penetrating a diamond crystal along the $\langle 100 \rangle$ axis. Furthermore, we ask for beam time with ultra relativistic heavy ions, as soon as CERN is able to deliver unbunched beams of these, to investigate nuclear size effects in a number of emission processes.

CERN-SPSC-2013-025 / SPSC-SR-122
07/10/2013

[1)] On behalf of the collaboration.

The results obtained in 2012 have been analysed, and 2 papers have been written, one of which is due to be published in Phys. Rev. D [5] and the other submitted for publication [6].

1 Structured target 'resonances'

1.1 2011 measurement

As described in [7], one of the aims of the 2011 run was to perform a dedicated experiment directed towards the detection of a so-called structured target resonance [2, 4, 3]. This gave a publishable result [1] which, however, left room for a more systematic study, based on resonances for several distances. In particular such a systematic investigation was desirable due to the lack of agreement with the unmodified theory of Blankenbecler [2] and that of Baier and Katkov [3], whereas good agreement with Blankenbecler's theory including a correction term $\overline{\delta}$ [4] was found. The correction term arises due to correlations between transverse coordinate amplitudes (with respect to the scattering centers) and the phase of the eikonal wave function, and is generally small for non-structured targets but gives a significant shift in 'resonance energy' for structured targets, corresponding to about a factor 2 in distance. Structured targets are thus attractive to verify the relevance of the correlation term in multiple scattering.

1.2 2012 measurement

Although experimentally little was left open for discussion - distances e.g. measured by three independent methods, each with few micron accuracy - the element of chance or mistakes of course could not be entirely ruled out, since essentially only one distance was measured in the 2011 experiment. We therefore in 2012 performed a more extensive investigation of the structured target resonances to investigate the significance of the correlation term and to obtain an accurate description of radiation emission in the presence of multiple scattering.

In a naïve approach, the resonance (or, rather, the lack of destructive interference) appears when the formation length

$$l_{\mathrm{f}} = \frac{2E(E-\hbar\omega)}{m^2c^3\omega} = \frac{2\gamma^2 c}{\omega^*} \qquad \omega^* = \omega\frac{E}{E-\hbar\omega}\,, \tag{1}$$

extends across the separation gap between two closely positioned foils. Thus, when the formation length equals the target spacing or gap width δg it leads to a resonance at a photon energy

$$\hbar\omega < \hbar\omega_{\mathrm{r}} = \frac{E}{1+\dfrac{\delta g}{2\gamma\lambda\!\!\!^{-}_c}}\,, \tag{2}$$

Other effects involving the concept of formation length may be found in [14, 15].

In order to avoid the problems associated with stacks of foils, we measured with only two foils, mounted on a precisely controlled translation stage, such that the internal separation between the two foils could be controlled with an accuracy of a few microns. This sets rather severe constraints on the amount of extra material in the beam, e.g. from thin trigger scintillators, vacuum-pipe windows and beam-line diagnostics such as wire-chambers. Furthermore, the requirement of measuring photon energies down to a few tens of MeV imposes constraints on the magnetic field applicable to deflect the electron from its radiated photon, due to the emission of typically several synchrotron radiation photons. To obtain a gentle deflection, i.e. a low field, two 2 meter long magnetic dipoles were run in series at a fairly low field, 0.17 T, giving a synchrotron radiation critical energy of $\hbar\omega_c = 3\gamma^3 e\hbar B/2p \simeq 3.6$ MeV. Even with pile-up originating from several synchrotron radiation photons being emitted simultaneously, this allows detection down to $\approx$ 30 MeV, without the need for deconvolution. Nevertheless, due to 'back-splash' from the lead glass calorimeter used to measure the energy of the electron, into the BGO calorimeter used to measure the energy of the photon, the lower detection limit was increased to $\approx$ 50 MeV, and the efficiency of the BGO found from reference measurements is considered reliable only above $\approx$ 100 MeV.

The effect becomes more pronounced if one plots the ratio between the structured target and the reference target as is done in Fig. 1. The background is subtracted from both spectra. Besides simulations based on the BD formulas, we also plot simulations based on the BD$-\delta$ formulas.

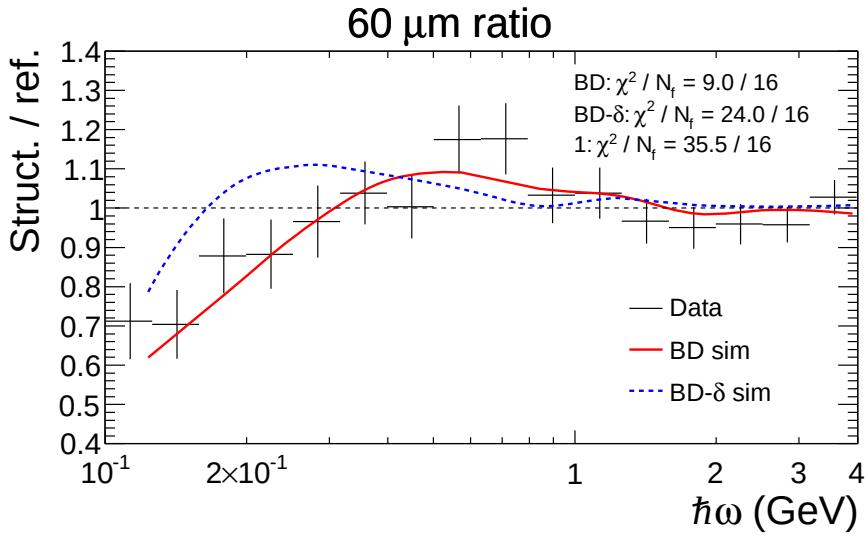

Figure 1: The ratio between the structured target and the reference target - both with the background subtracted. For the data markers, the vertical bars indicate the statistical error bars and the horizontal bars are the bin width. The solid red lines are simulations based on the BD formulas and the dashed blue lines are based on the BD−δ formulas.

As shown in figure 1, adapted from [6], there is quite good agreement between theory and measured values for the ratio between the radiation spectra (after background subtraction) obtained with 178 GeV electrons passing 2 foils of each 26 micron thick gold, at separations of nominally 60 microns and 20 mm. Using the ratio as the observable eliminates many systematic effects, but also the spectra by themselves (not shown) are in good agreement with theory, including LPM and TSF effects (for these effects, see [19, 1]). Clearly, there is an effect of increasing the distance between the foils, and already from these data we can conclude that formation lengths for $\simeq$ 1 GeV photons emitted by multi-GeV electrons can be measured directly, in effect by means of a micrometer screw.

These findings are interesting, since a previous experiment on structured targets [1] had a preference for the BD−δ theory. After re-analyzing this experiment, it was found that one of the cuts used on the data had a significant bias towards low photon energies. When this was corrected, the data were consistent with both the BD, BD-δ and no effect, but with a slight preference for the BD theory. Similarly, measurements on thin targets [16] and the LPM effect [6] also have a preference for the BD theory. One is therefore tempted to question the validity of the BD−δ theory.

These are the first measurements to observe the gap dependence of the energy of the shoulder in the radiation spectrum from a structured target on a truly macroscopic scale up to 0.5 mm which is fascinating when comparing to the photon wavelength of just 10 femtometers. The results are compared to the theories of Blankenbecler and Drell and found to be in favour of their first, unmodified results, in contrast to previous measurements.

From the ratios such as the one plotted in Fig. 1 we have determined the position of the peak, $\hbar\omega_p$. This establishes the connection between the formation length of the photon and the position of the peak in the radiation spectrum. For the BD theory the agreement is good, as expected from the earlier figure, and the peak is positioned at energies substantially higher than for the BD-δ theory. The estimate of Baier and Katkov (BK), is roughly a factor of 2.3 below Eq. (2) and significantly below our data. The agreement of BK with the BD−δ theory is possibly accidental, since the estimate agrees with the BD calculations in other cases [3]. This is at least partially due to a $1/l_t^2$ dependence for $\hbar\omega_{p,BK}$ and only $1/l_t$ for $\hbar\omega_p$.

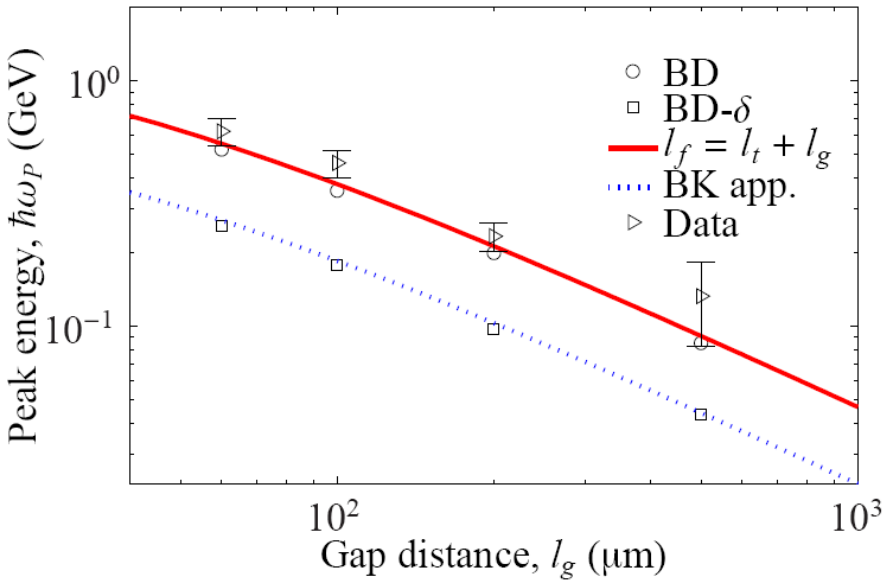

Figure 2: The position of the peak in the radiation spectrum as a function of the gap size l_g. The red line is Eq. (2). Adapted from [6].

2 Landau-Pomeranchuk-Migdal effect for low-Z targets

The Landau-Pomeranchuk-Migdal (LPM) effect was investigated experimentally in the mid-90s with 25 GeV electrons at SLAC [21] and later with up to 287 GeV electrons at CERN [22, 23]. These investigations - combined with relevant theoretical developments - have shown that the theory of multiple scattering dominated radiation emission is describing experiment very well, at least for high-Z targets.

In his review paper on the LPM effect from 1999 [24], Spencer Klein stated among the explanations for a small, but significant discrepancy found for carbon with electrons at 25 GeV that "'it is also possible that Migdaløs theory may be inadequate for lighter targets."'. Likewise, in the CERN experiments [23], where carbon was used as a calibration target, the systematic deviations from the expected values for E_{LPM} could possibly be explained by an insufficient theoretical description of carbon.

As described in [20], the most widely used theory for the LPM effect, developed by Migdal [25], potentially has at least two shortcomings: It is based on the Thomas-Fermi approximation, known to be inaccurate for atoms of low nuclear charge [25, eq. (22)], and for several combinations of electron energies and photon energies, the resulting spectra show what seems to be an unphysical 'kink' in the radiation spectrum. The aim of our measurements in 2012 was to address these questions.

Moreover, the more modern theory by Baier and Katkov which includes Coulomb corrections and other fine details, is developed mainly for high-Z targets, and therefore does not include screening adequately for low-Z targets. The accuracy of their theory is expected to be a few percent for high-Z targets, and substantially worse for low-Z targets. Nevertheless, their theory almost exactly (within about 2% over 5 orders of magnitude in photon energy) reproduces the theory of Migdal for e.g. 178 GeV electrons passing a 2% X_0 carbon target.

Finally, the contribution from electrons may be influenced differently by the LPM effect than the nuclear contribution, resulting in another potential difference between the true multiple scattering effects in low-Z and high-Z targets.

Therefore, a measurement of the LPM effect in low-Z targets was warranted. Thus, we have addressed the question of the potential inadequacy of the commonly used Migdal formulation of the Landau-Pomeranchuk-Migdal (LPM) effect by measuring the photon emission by 20 and 178 GeV electrons in the range 100 MeV - 4 GeV, in targets of LowDensityPolyEthylene (LDPE), C, Al, Ti, Fe, Cu, Mo and, as a reference target, Ta. For each target and energy, a comparison between simulated values based on the LPM suppression of incoherent bremsstrahlung was performed, taking multi-photon effects into account. For these targets and energies, we found that Migdal's theoretical formulation is adequate

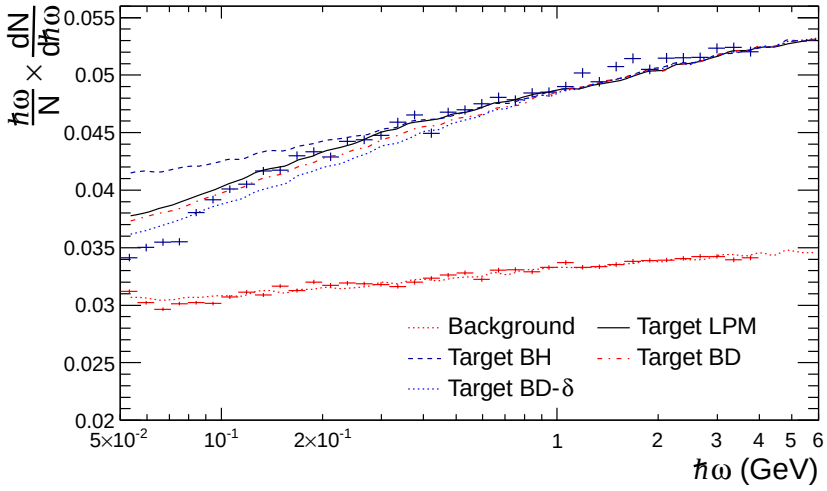

Figure 3: Power spectrum of radiation emission from 178 GeV electrons penetrating carbon. The spectrum is normalized to the number of incoming electrons. The lower, red dotted line shows the simulated contribution from the background, with data points representing the values obtained in the experiment. The middle, blue line shows the simulated contribution from the targets, including the LPM effect, and with data points representing the values obtained in the experiment. The upper, black dashed line shows the simulated contribution from the targets, excluding the LPM effect. Only statistical uncertainties are shown. Furthermore is included simulations based on the BD and BD−δ theory. Adapted from [5].

to a precision of better than about 5%, irrespective of the target substance.

For the reference targets of aluminum and tantalum there is generally a good agreement between data and simulated values (for Ta only when including the LPM effect, as expected), except perhaps for the lowest (intermediate) photon energies 50-120 (120-600) MeV for the Al (Ta) target where a $\simeq$ 5% discrepancy is seen. The discrepancy below 100 MeV may be attributed to influence from the synchrotron radiation and/or backsplash in the BGO.

There is a slight tendency for the data to be a steeper function of photon energy than the simulated values. For aluminum and titanium there is again good agreement with simulations including the LPM effect, except for a small systematical shift of experimental values below about 400 MeV. For iron and copper targets - with very similar atomic numbers - the spectra are close to being identical with an indication of a change of slope at the $\simeq$ 5% level. Finally, for the medium $Z = 42$ molybdenum, the data points are consistently 5-10% higher than the simulated values including the LPM effect, indicating a systematic error.

As an example, in Fig. 3 we show the results for carbon where we have also calculated the spectrum for the BD and BD−δ theory. In the energy interval from 100 MeV to 1 GeV where the theories differ we have calculated the χ^2 value. The number of degrees of freedom is 20 and $\chi^2_{\text{Migdal}} = 28$, $\chi^2_{\text{BD}} = 69$ and $\chi^2_{\text{BD}-\delta} = 209$. In other words the data have a preference for the Migdal formula. There is a slight disagreement with the BD curve and the BD−δ curve is consistently below our data.

3 Plans for 2014

4 Positron production by electrons in a diamond

In view of recent developments in the field of efficient positron production by use of crystalline targets [27, 28, 29, 30, 31], we have on previous occasions [20, 7] shortly described a possible study using diamond crystals. The relevance of such a study is high, as e.g. CLIC and LHeC e^+-production schemes are expected to gain significantly (at least several tens of percent, perhaps even factors of 3-4) from using crystalline targets where the strong field effects - studied in detail experimentally by the NA43 and NA63 collaborations - play a decisive role. Due to the high power of the primary electron beam in such schemes, characteristics such as radiation hardness, melting point and thermal conductivity of the target are key elements. Diamond is unique in this respect, known to be superior to all other crystals, but clearly has the disadvantage of high cost, in particular for large specimens.

From prof. M. Winter, Strasbourg, we have bought 11 of the so-called MIMOSA-26 detectors [32], CMOS-based position sensitive detectors with 1152 columns of 576 pixels, $\simeq$ 18.4 μm pitch, readout in 110 ms, $\simeq$ 3.5 μm resolution and true multi-hit capability (at least 20 charged particles per read-out). In 2012 we had acquired 5 (one of which broke) and the remaining ones will be acquired soon. Thus, in 2012 we reduced the setup to a test of the principle of operation of the magnetic pair spectrometer configuration.These detectors are approximately 1×2 cm^2 (two of them are 'doubles', i.e. approximately 2×2 cm^2) and represent only the material of $\simeq$ 50 μm of silicon to the beam, i.e. $\Delta t/X_0 \simeq 0.05\%$ each. The production angles and energies can be measured by means of the MIMOSA detectors arranged in a magnetic spectrometer configuration with a permanent-magnet-based magnetic dipole that through a shunting mechanism has a variable field (the dipole was kindly provided on loan from DANFYSIK). The advantage of a permanent-magnet-based magnetic dipole is naturally its lack of power consumption that makes it possible with relative ease to install the entire spectrometer configuration in vacuum - no need for water cooling nor current supply. We plan to do this in future measurements, giving a significantly improved momentum resolution at the low pair energies (few tens of MeV) which are of main interest.

A photograph of the setup is shown in figure 4. With a 1.5 mm thick single crystal diamond aligned along the $\langle 100 \rangle$ axis as target, a first test setup of the positron-production in diamond has been done. Unfortunately the off-line analysis has shown that generating tracks between the MIMOSA detectors yields very few good events, most likely due to a too low efficiency of each detector. For 2014, the track-finding will be essentially online to solve the non-trivial task of setting the optimum efficiency, since the number of noise-hits (inherent to the MIMOSA-technology) rises fast with increasing efficiency.

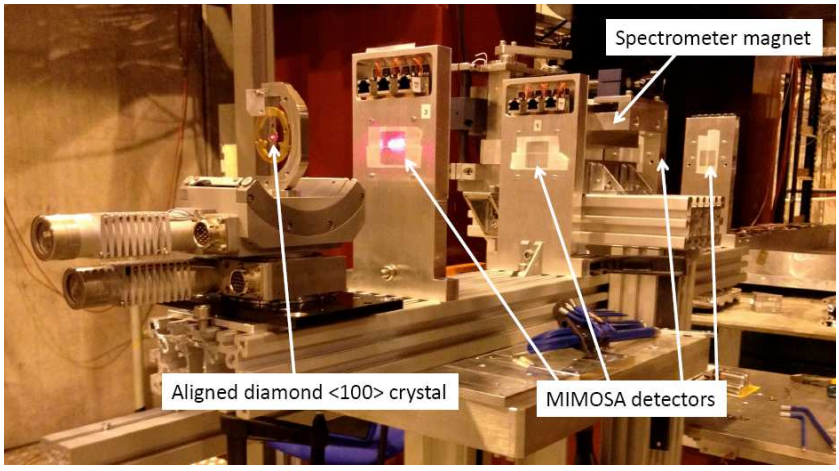

Figure 4: *MIMOSA-setup*

We have found that previous measurements using diamond have been performed, but with a somewhat different setup that only allows measurements at specifically chosen positron momenta and integrated over forward angles [33]. In those measurements the enhancement is high for diamonds of small thicknesses, whereas for thicknesses large enough to yield an acceptable production rate the enhancement for diamond is smaller than for other crystals, and fairly rapidly approaches one, with increasing

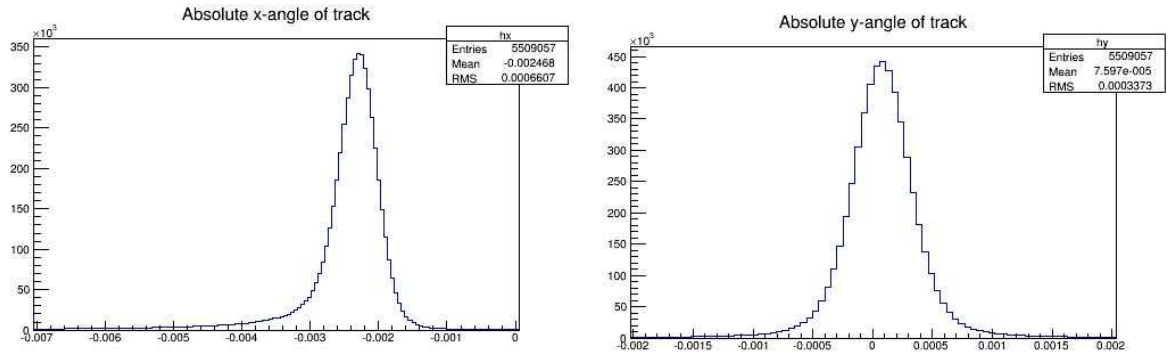

Figure 5: Histogram of deflection angle in horizontal and vertical directions. The angle is given in radians.

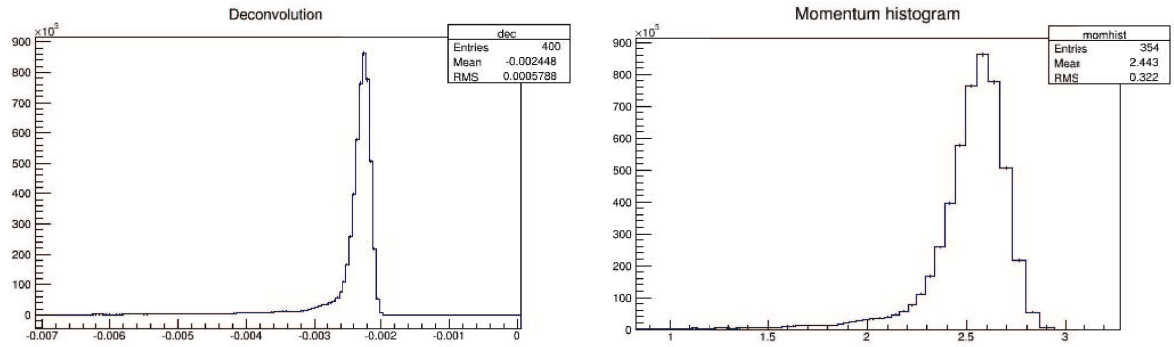

Figure 6: The scattering in the x-direction deconvoluted with the scattering in the y-direction and a momentum histogram from the 2.5GeV DESY run.

thickness. It must be emphasized, though, that the actual phase-space density has not been measured, the enhancement thus likely being a pessimistic number.

4.1 MIMOSA test at DESY

In order to gain understanding of the analysis procedure for the MIMOSA detectors, we participated in a CLIC detector testbeam at DESY, where they have 6 MIMOSA detectors set up permanently. These are used for testing other devices to be placed between the two sets of 3 planes. We placed a permanent dipole magnet there and got data that allowed us to measure the beam momentum. The output file format from the DESY testbeam is different than what we use, but the output we got was just the coordinates of the hits in the detectors. The software developed from this test is therefore also usable on our own data. Based on this data we wrote the software that finds tracks in the first 3 planes and the last 3 planes, and which then finds the deflection of the tracks. We are therefore able to measure the energy of the beam, and use this as a test of the software to be used in 2014. In figure 5 are plots of the deflection angle of the particles in the horizontal (x) and vertical (y) direction for the run with largest number of events from the DESY testbeam. The energy was tabulated as 2.0GeV but due to an error on DESY's part, the delivered energy was 25% too high, due to a bending magnet set at the wrong current. This was in fact realised also through our measurements, which showed an energy of 2.5GeV.

We have implemented a deconvolution routine to reduce the effect of multiple scattering. The distribution of scattering in the x-direction is deconvoluted with the distribution of scattering in the y-direction, which gives us the deflection distribution purely due to the magnet. A momentum histogram is then obtained from the correspondence between deflection angle and momentum - see figure 6.

As seen from the momentum histogram, there is good agreement between the measured and the expected momentum value. We have thus demonstrated that we can make accurate measurements of momentum distributions using such a setup.

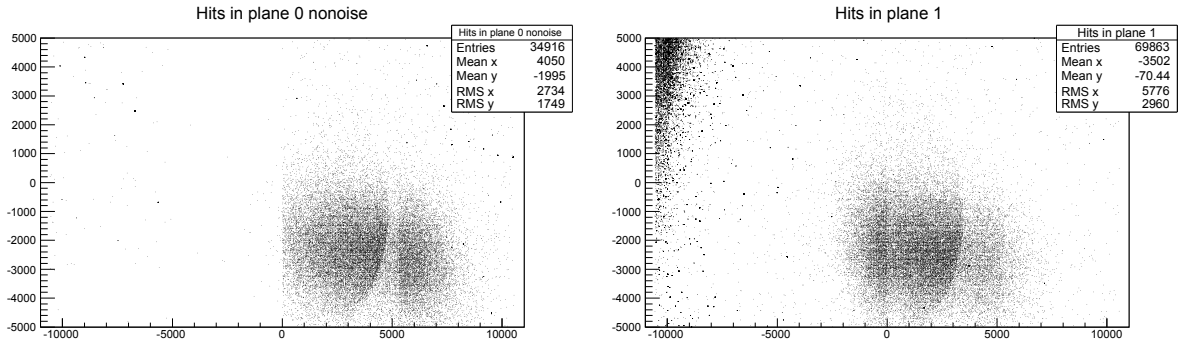

Figure 7: The figures on the left and right show the hits in plane 0 and 1, after removal of noisy pixels.

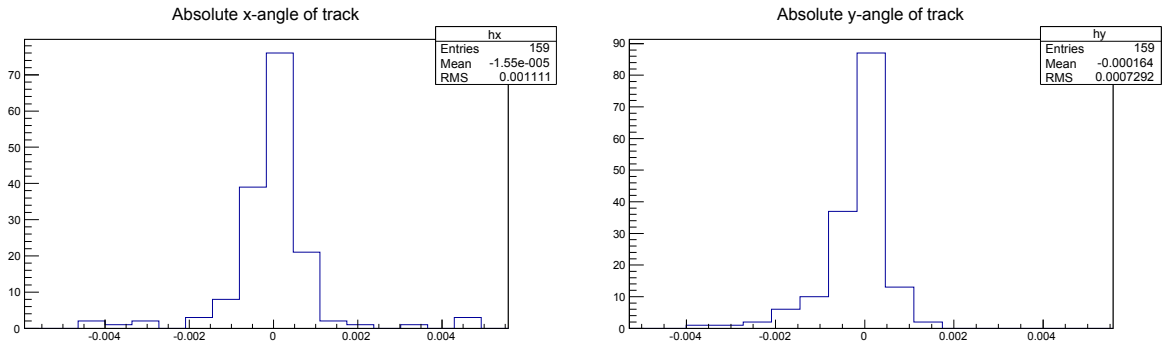

Figure 8: The deflection in x and y directions of the tracks found.

4.2 Results from the initial test in 2012

Upon the beginning of the analysis of the data from the initial test, using 2 days of beam time in 2012, it was apparent that there was a problem with the calibration of the detectors. See figure 7

The left half of the first detector (plane 0) was unresponsive, but was positioned such that the beam was mostly in the right half. In plane 1, 2 and 3, there are hits in the upper left corner, not caused by particles. We have afterwards reproduced this with the detectors running without beam. The above data is from 10^6 events, and thus we would expect 10^6 entries in these histograms in contrast to the 3.5×10^4 seen. This can be caused by faulty triggering or low detection efficiency of the MIMOSA detectors. Applying the same analysis routines that worked well with the DESY data reveals the results seen in figure 8. The very low number of tracks from 5.5×10^6 events, indicates a low detection efficiency of the MIMOSA detectors, since the number of hits in each plane is a lot larger than the number of tracks found. Assuming the problem to stem only from the detection efficiency of the MIMOSA detectors gives us that we had only 17% of the incoming particles generated a hit.

After the discovery of the faulty calibration, we have recalibrated the detectors at Aarhus using a radioactive β-source. A beam-test planned for week 46, 2013, is dedicated to solving the problems related to (in)efficiency.

4.3 Theoretical predictions of the pair production rate

We have theoretical simulations under way to accurately predict the energy and angular distribution of the produced pairs from electrons of 10GeV channeled axially along the $\langle 100 \rangle$ axis of diamond. Such a calculation is not completely trivial, in particular the calculation of the radiation emission of the electron: There are two angles that characterize the problem: The particle's angle with the crystal axis, when in the center of the potential, given by $\theta_U = \sqrt{\frac{2U_0}{m\gamma}}$, where $U_0 = 103$ eV is the depth of the potential for diamond. And the characteristic angle of radiation emission $\theta_{rad} = \frac{1}{\gamma}$.

When $\frac{\theta_{rad}}{\theta_U} \ll 1$ or $\frac{\theta_{rad}}{\theta_U} \gg 1$, simplifying approximations can be made to solve the problem. But in our case we have $\frac{\theta_{rad}}{\theta_U} \simeq 2.8$, and thus the problem must be solved without making any approximations,

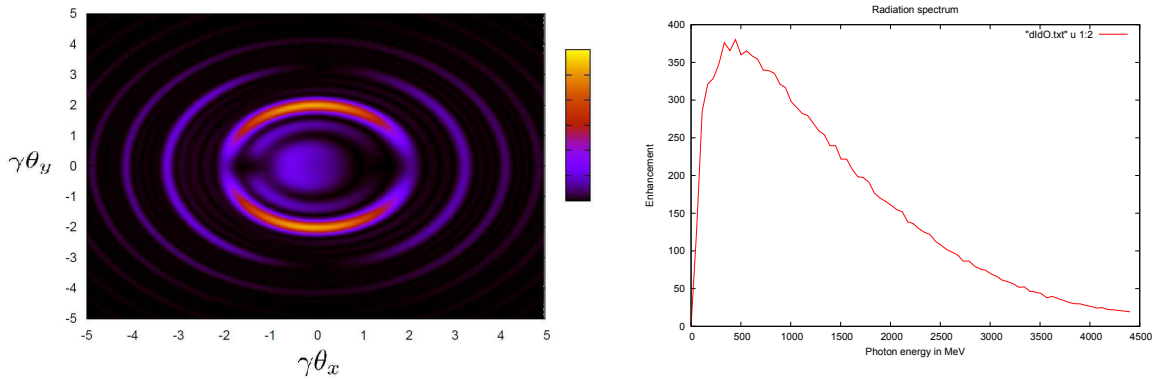

Figure 9: To the left is the angular distribution of radiation at a frequency of 2 GeV in arbitrary units. To the right is the averaged intensity distribution in photon frequency for 10 GeV electrons in a string potential with an entry angle of $\theta = 0$ to the axis.

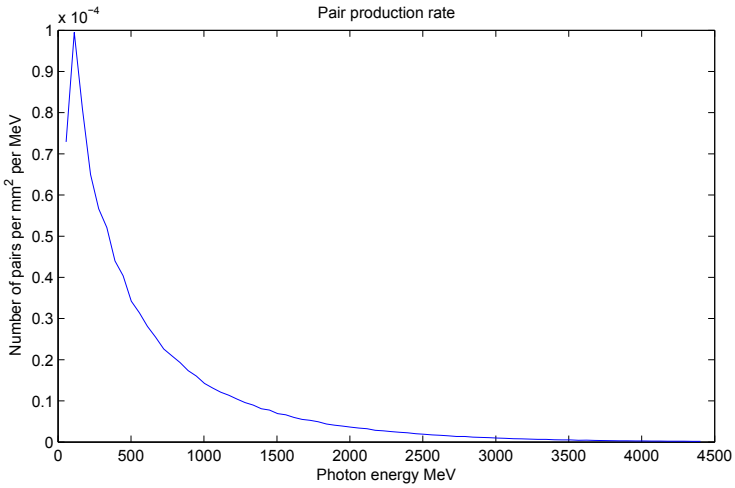

Figure 10: Number of pairs per mm^2 per MeV. Since the pair production in targets thicker than the photon formation length is dominated by 'sequential' tridents [10, 17], where the intermediate step is a real photon, the dependence on the thickness is quadratic.

by simply finding the trajectory of each particle, and using the formula

$$\frac{d^2I}{d\omega d\Omega} = \frac{\alpha}{4\pi^2}\left|\int_{-\infty}^{\infty} \frac{\boldsymbol{n}\times[(\boldsymbol{n}-\boldsymbol{\beta})\times\dot{\boldsymbol{\beta}}]}{(1-\boldsymbol{n}\cdot\boldsymbol{\beta})^2} e^{i\omega\frac{E}{E-\omega}(t-\boldsymbol{n}\cdot\boldsymbol{r}(t))}dt\right|^2, \tag{3}$$

for each of them. Here $\boldsymbol{n}$ is the direction of observation, $\boldsymbol{\beta} = \frac{\boldsymbol{v}}{c}$, α the finestructure constant and ω the photon frequency. Even though the electron energy of 10 GeV is small with respect to the quantum strong field effects, it is a noticeable correction for particles with an amplitude of half of the maximum, or less. Solving this problem is computationally tedious, and therefore we have implemented a software routine using the Nvidia CUDA library for C++, which allows one to utilize the multithread power of a GPU to make fast calculations. Once the radiation distribution has been calculated, the pair production rate can be found.

At the moment we have only calculated the differential pair production with respect to the energy of the photon from which the pair was created, to determine the required measurement time see 10. Full calculations of the distribution with respect to the electron/positron energy and angular distribution to be compared with the measurements are expected to be ready within the coming few months.

Integrating this over the photon frequency gives approximately $4.9 \cdot 10^{-2}\text{mm}^{-2}$ pairs per incom-

ing electron. For the 'random' (non-aligned) configuration, the rate is approximately $1.7 \times 10^{-3}\text{mm}^{-2}$, indicating an enhancement of a factor $\simeq 30$.

4.4 Requested beam and beam time

With a 1.5 mm thick diamond, a production rate of $4.9 \cdot 10^{-2}\text{mm}^{-2}$ and a burst rate of $3 \cdot 10^{4}$Hz, 1 burst per minute (including down-time of the accelerator, estimated to be 25%), this corresponds to 3.2 million positrons produced per day. Expecting to divide this data set into 20 bins in both energy and angle, this equals 8000 positrons per bin per day, such that a measurement of the aligned crystal can be done in 2 days. However, also a no-target and a 'random' (non-aligned) crystal measurement must be performed with good statistics, both of which require about twice the time for each, due to the lower production rate. Furthermore, in order to enable a reliable extrapolation to the 5 GeV electrons planned to be used for the CLIC injector positron production, we need to measure at 10 (the lowest energy achievable in SPS H4), 20 and 50 GeV. Thus, the full data taking time is expected to be 18 days. Setting up and beam tuning is expected to be possible to finish in 3 days.

Summarizing, we request 3 weeks of beam time in SPS H4, for the measurement of pair production from diamond. The requested beam is electrons with a peak rate of a few 10^{4}Hz at energies of 10, 20 and 50 GeV, and with a small divergence, preferably 100 μrad.

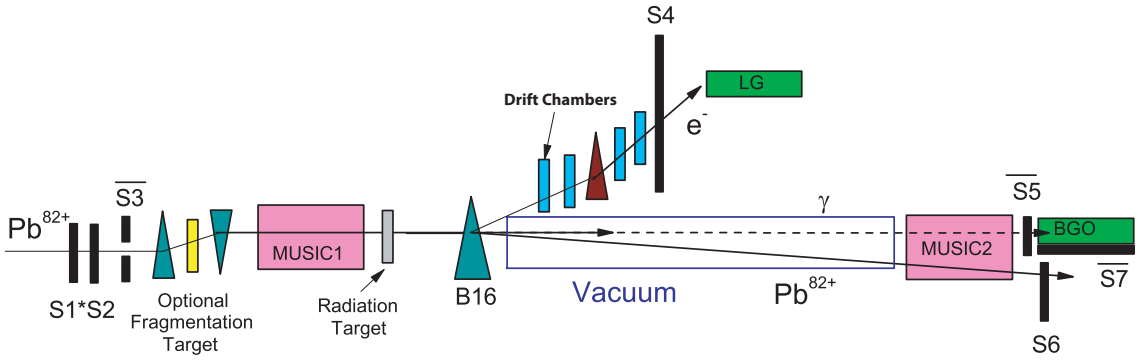

Figure 11: *A figure showing the proposed setup. The Pb^{82+} ions are incident from the left, through three thin scintillators - two counters S1 and S2 and one veto with a hole S3 - to the removable fragmentation target. The fragmentation target enables investigations of radiation emission from fragments, the charge state of which are found by MUSIC1. The ions then impinge on the radiation target. After this target, the ions are deflected using a 4 Tm magnetic dipole field (B16, MBPL installed in H4) into MUSIC2 where the charge state of the spent ion can be detected. Produced $\delta-$electrons are deviated into scintillator S4. Finally, the emitted photon is intercepted by a BGO (for energies 0.1-2 GeV) or lead glass (for energies 2-200 GeV) calorimeter, where S5 is a veto for events where the photon has converted. The deviated ions are counted in S6, and S7 is installed to avoid events with backsplash from the ions into the calorimeter.*

5 Nuclear-size effects in emission processes

In addenda to our proposal [12, 20, 7] we have proposed to measure the bremsstrahlung emission from $\gamma = 170$ Pb^{82+}. As previously reported, our setup has been mechanically and electronically tested in 2011 and proven to be well-functioning, and a more elaborate setup is therefore planned for the first availability of *debunched* $\gamma = 170$ Pb^{82+} ions in SPS H4. An overview of the proposed setup is shown in figure 11. The setup offers several new possibilities discussed earlier [12, 20, 7] and here mentioned briefly:

Bremsstrahlung from Pb^{82+}

Bremsstrahlung from nuclei with $Z \neq 82$

'Bruchstrahlung' from collisions with nuclear breakup/fragmentation $Z = 82 \rightarrow Z \neq 82$

Delta-electron intensity and effects caused by the finite nuclear size

As the first three items on this list have been described in detail in previous reports, we here focus on the delta-electrons.

5.1 Emission of delta-electrons

Generally, the energy of delta-electrons is limited by $T_{\max}$ given by

$$T_{\max} = \frac{2\gamma^2\beta^2 m_e c^2}{1 + 2\gamma m_e/M + (m_e/M)^2} \simeq 2\gamma^2\beta^2 m_e c^2 \tag{4}$$

where the last approximation - although typically described as the 'low-energy' approximation - in the present connection is sufficient for all practical purposes. However, the result eq. (4) is derived for a point-like projectile and the finite size of the nucleus leads to a quite different emission spectrum and an effective maximum energy that is significantly lower (although kinematically still given by eq. (4)).

Upon a change to the rest frame of the ion (practically the same as the center-of-mass frame) in which the electron is incident on the ion the de Broglie wavelength $\lambda\!\!\!^{-} = \hbar/p$ of the incident electron becomes comparable to the radius of the nucleus R, i.e. $\chi \equiv R/\lambda\!\!\!^{-}$ becomes larger than 1 [8]. Thus, the electron will 'feel' the constituents of the ion and therefore not register it as a point-like object of charge Ze (in a sense similar to the virtual photons in the emission of bremsstrahlung).

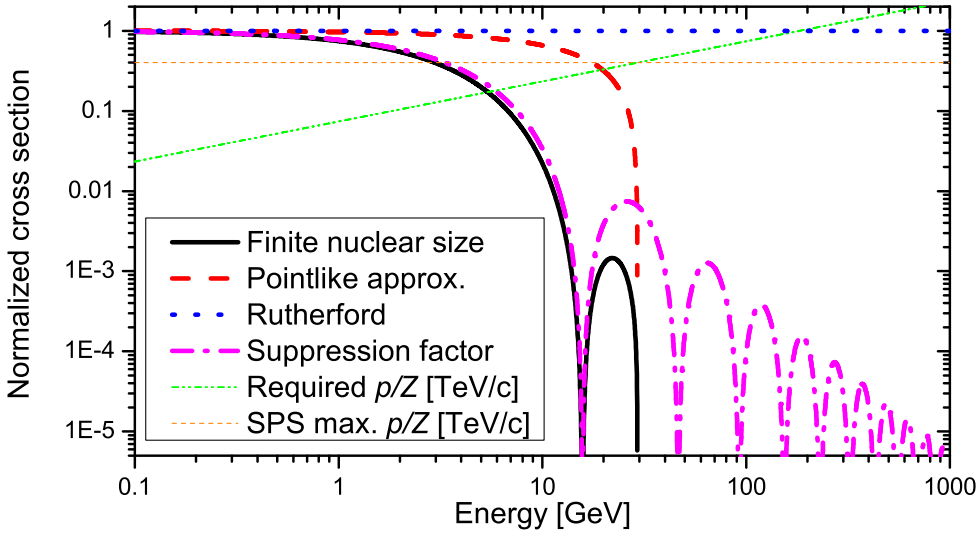

Figure 12: *Calculations for the generation of delta-electrons as a function of their energy in GeV, using* Pb^{82+}. *The thick lines show calculations of the normalized cross sections* $\omega^2 d\sigma/d\omega$ *for* $\gamma = 170$ *based on the finite nuclear size, homogeneously charged sphere (black, full), the point-like approximation (red, dashed) and the Rutherford cross section,* $2\pi Z^2 r_e^2/\beta^2 \simeq Z^2 \cdot 0.5$ *barn (blue, dotted) [8]. The additional thick line is the suppression factor, i.e. the ratio between the finite nuclear size and the point-like approximation, which only depends on the energy of the* Pb^{82+} *projectile through its corresponding maximum energy transfer to the delta-electrons (purple, dash-dotted). The thin lines show the required momentum per charge in TeV/c of the* Pb^{82+} *projectile, to generate delta-electrons with the corresponding maximum energy (green, dash-dot-dotted) and the maximum momentum per charge in TeV/c of the* Pb^{82+} *presently available at the CERN SPS.*

In figure 12 is shown calculations based on [8] for the generation of delta-electrons as a function of their energy in GeV, using Pb^{82+} projectiles. With thick lines is shown the normalized cross sections $\omega^2 d\sigma/d\omega$ for $\gamma = 170$ based on the finite nuclear size, homogeneously charged sphere, the point-like approximation and the Rutherford cross section. The additional thick line is the suppression factor, i.e. the ratio between the finite nuclear size and the point-like approximation. The suppression factor only depends on the energy of the Pb^{82+} projectile through its corresponding maximum energy transfer to the delta-electrons as found from eq. (4). The thin lines show the required momentum per charge in TeV/c of the Pb^{82+} projectile, to generate delta-electrons with the corresponding maximum energy (green, dash-dot-dotted) and the maximum momentum per charge in TeV/c of the Pb^{82+} presently available at the CERN SPS (orange, dashed). The two latter curves cross around 400 GeV/Z where the suppression factor at the maximum energy of the delta-electrons, $T_{\max} = 29.3$ GeV, is $\simeq 150$. However, near this energy the number of delta-electrons becomes very low. From an experimentalist point of view, a more realistic scenario is to use 200 GeV/Z Pb^{82+} (where also safety issues related to the extraction procedure are simpler to solve), with $T_{\max} = 7.3$ GeV focusing on the region of delta-electron energies around 4 GeV where the suppression factor is $\simeq 3$ and the drop in cross section compared to the Rutherford value is only a factor $\simeq 2$. Due to the different spectral shapes, combined with the difference in total cross section, a few points measured around 4 GeV would enable a distinction between the point-like model, and that of the finite nuclear size. This is the aim of the measurement proposed, but since the upper end of the delta-electron spectrum is very sensitive to the exact model for the charge distribution [8], it can be envisaged to investigate this further in the future.

The delta-electrons are easily bent out of the beam to a position where position-sensitive detectors can measure their energy. Since the high energy delta-electrons are produced at small emission angles, they can all be measured simultaneously. Hence, the high energy differences in cross section can be studied with very good accuracy. The low energy delta-electrons are scattered slightly more, and a larger detector is therefore appropriate. We therefore propose to use the well-tested Drift Chambers to do a

first measurement of the charge distribution of the lead nucleus using the emitted delta-electrons. In figure 13 and 14 are shown simulations of the intensity of delta-electrons impinging on a drift chamber, for two different nuclear charge distribution models: point-like nucleus and a homogeneously charged sphere. The simulations shows intensities achievable with approximately 1 week of beam time. Clearly, the point-like distribution can be distinguished from the others, whereas the distinction between the homogeneously charged sphere and the Fermi distribution requires significantly more statistics.

With a positive result we can turn to a more precise MIMOSA-based measurement that can probe the cross section differences at high energy and ultimately test the homogenous charge distribution hypothesis against the Fermi distribution hypothesis.

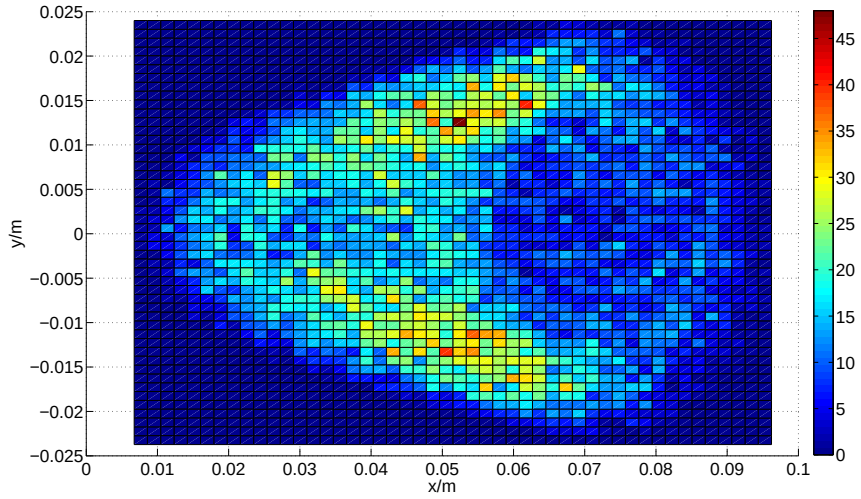

Figure 13: *Monte Carlo simulation of detected delta-electrons during approximately* 1 *week of measuring. This result is calculated in the point approximation for the nuclear charge. The plot shows the position of delta-electrons* 1.5 *m downstream of target after having passed through an integrated magnetic field of* 1 *Tm. The lead beam is centered at (x,y) (0,0).*

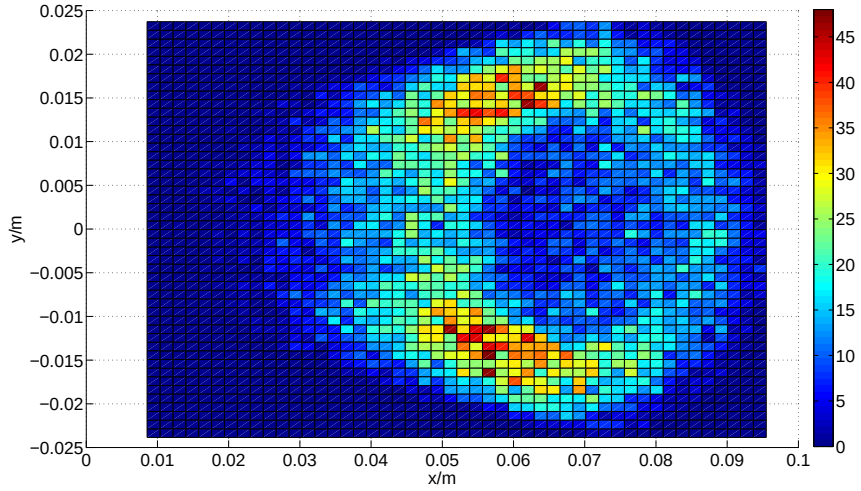

Figure 14: *Monte Carlo simulation of detected delta-electrons during approximately* 1 *week of measuring. This result is calculated using a homogeneous distribution of the nuclear charge.*

The strongest signals for the proposed measurements are expected for Pb ions. However, smaller ions, down to Ar, are also expected to generate a detectable effect.

The method allows - essentially through a change of reference frame - investigations of the nuclear charge distributions using the electrons present in a solid. The strength of it is that in contrast to measurements using electrons impinging on stationary ion targets, it opens for the possibility to measure charge distributions for elements with a short half-life (down to a few hundred nanoseconds), e.g. for fragments generated in the beam line.

5.2 Requested beam and beam time

Due to the presence of the MUSIC detectors, which operate with a time-scale of a few microseconds, the proposed setup cannot accomodate more than about 10^5 particles per burst. Moreover, the beam has to be actively debunched before extraction from the SPS (as it was done in previous runs before 2010), since projectiles arriving at the detectors with a separation time shorter than a few microseconds, means that the event has to be discarded.

The need for a long lever arm to efficiently separate the lead ion from the radiation it has emitted, given a maximum bending power of the MBPL magnets of about 4 Tm, means that the experiments can only be performed in SPS H4. In H8, for example, there are no available zones where an MBPL can be installed with 50 metres of free space downstream (extending from zone PPE134 into PPE144 as was done in 2011).

We request 2 weeks of beam time with fully stripped ions of a species in the range between Ar and Pb with 3-4 momenta per charge in the range from $p/Z = 30$ GeV/c to as high as safety issues allow it, preferably at least to $p/Z = 200$ GeV/c. Since active debunching is required, we ask for CERN to allocate the beam time as soon as such a beam becomes available.

6 Status of publications and theses

Publications and theses related to the activities of NA63:

1. T. Virkus, U.I. Uggerhøj, H. Knudsen, S. Ballestrero, A. Mangiarotti, P. Sona, T.J. Ketel, A. Dizdar, S. Kartal and C. Pagliarone (CERN NA63): *Direct measurement of the Chudakov effect*, Phys. Rev. Lett. **100**, 164802 (2008)
2. A. Mangiarotti, S. Ballestrero, P. Sona and U.I. Uggerhøj: *Implementation of the LPM effect in the discrete-bremsstrahlung simulation of GEANT 3 and GEANT 4*, Nucl. Instr. Meth. B **266**, 5013 (2008)
3. H.D. Thomsen, K. Kirsebom, H. Knudsen, E. Uggerhøj, U.I. Uggerhøj, P. Sona, A. Mangiarotti, T.J. Ketel, A. Dizdar, M. Dalton, S. Ballestrero and S. Connell (CERN NA63): *On the macroscopic formation length for GeV photons*, Phys. Lett. B **672**, 323 (2009)
4. J. Esberg and U.I. Uggerhøj: *Does experiment show that beamstrahlung theory - strong field QED - can be trusted?*, Journal of Physics Conference Series, **198**, 012007 (2009)
5. J. Esberg, K. Kirsebom, H. Knudsen, H.D. Thomsen, E. Uggerhøj, U.I. Uggerhøj, P. Sona, A. Mangiarotti,, T.J. Ketel, A. Dizdar, M. Dalton, S. Ballestrero, S. Connell (CERN NA63): *Experimental investigation of strong field trident production*, Phys. Rev. D **82**, 072002 (2010)
6. K.K. Andersen, J. Esberg, K.R. Hansen, H. Knudsen, M. Lund, H.D. Thomsen, U.I. Uggerhøj, S.P. Møller, P. Sona, A. Mangiarotti, T.J. Ketel, A. Dizdar and S. Ballestrero (CERN NA63): *Restricted energy loss of ultrarelativistic particles in thin targets - a search for deviations from constancy*, Nucl. Instr. Meth. B **268**, 1412 (2010)
7. H.D. Thomsen, J. Esberg, K.K. Andersen, M. Lund, H. Knudsen, U.I. Uggerhøj, P. Sona, A. Mangiarotti, T.J. Ketel, A. Dizdar, S. Ballestrero and S.H. Connell (CERN NA63): *Distorted Coulomb field of the scattered electron*, Phys. Rev. D, **81**, 052003 (2010)
8. H.D. Thomsen and U.I. Uggerhøj: *Measurements and theories of the King-Perkins-Chudakov effect*, Nucl. Instr. Meth. B, **269**, 1919 (2011)
9. A. Mangiarotti, P. Sona, S. Ballestrero and U.I. Uggerhøj: *A general semi-analytic method to simulate discrete bremsstrahlung at very low radiated photon energies by the Monte Carlo method*, Nucl. Instr. Meth. B, **269**, 1977 (2011)
10. A. Mangiarotti, P. Sona, S. Ballestrero, K.K. Andersen and U. I. Uggerhøj: Comparison of analytical and Monte Carlo calculations of multi-photon effects in bremsstrahlung emission by high-energy electrons, Nucl. Instr. Meth. B **289** 5-17 (2012)
11. K.K. Andersen, S.L. Andersen, J. Esberg, H. Knudsen, R. Mikkelsen, U.I. Uggerhøj, P. Sona, A. Mangiarotti, T.J. Ketel and S. Ballestrero (CERN NA63): Direct measurement of the formation length of photons, Phys. Rev. Lett. **108** 071802 (2012); see also accompanying Physics Synopsis and Science Daily.
12. K.K. Andersen, J. Esberg, H. Knudsen, H.D. Thomsen, U.I. Uggerhøj, P. Sona, A. Mangiarotti, T.J. Ketel, A. Dizdar and S. Ballestrero (CERN NA63): Experimental investigations of synchrotron radiation at the onset of the quantum regime, Phys. Rev. D **86**, 072001 (2012)
13. K.K. Andersen, J. Esberg, H.D. Thomsen, U.I. Uggerhøj and S. Brock: Radiation emission as a virtually exact realization of Heisenbergs microscope, Nucl. Instr. Meth. B, in press (2013)
14. U.I. Uggerhøj: Crystals, critical fields, collision points and a QED analogue of Hawking radiation, in W. Greiner (ed.): Exciting Interdisciplinary Physics, Springer Verlag (2013)
15. J. Esberg, U.I. Uggerhøj, B. Dalena and D. Schulte: Strong field processes in beam-beam interactions at CLIC, subm. to. Phys. Rev. Spec. Top. Acc. Beams (2013)
16. K.K. Andersen, S.L. Andersen, J. Esberg, H. Knudsen, R. Mikkelsen, U.I. Uggerhøj, T.N. Wistisen, A. Mangiarotti, P. Sona and T.J. Ketel (CERN NA63): Experimental investigation of the Landau-Pomeranchuk-Migdal effect in low-Z targets, Phys. Rev. D, accepted for publication (2013)
17. K.K. Andersen, S.L. Andersen, J. Esberg, H. Knudsen, R. Mikkelsen, U.I. Uggerhøj, T.N. Wistisen, A. Mangiarotti, P. Sona and T.J. Ketel (CERN NA63): Experimental measurement of radiation effects caused by the macroscopic dimension of the formation length, subm. to Phys. Rev. Lett. (2013)
18. T.N. Wistisen and U.I. Uggerhøj: Vacuum birefringence by Compton backscattering through a strong field, Phys. Rev. D **88** 053009 (2013)

19. H.D. Thomsen, Taming GeV photons and antimatter, Ph.D. thesis, Aarhus University 2010
20. U.I. Uggerhøj - Ultrarelativistic particles in matter, Doctoral dissertation, Aarhus University 2011
21. J. Esberg - An experimental approach to simulations of the CLIC interaction point, Ph.D. thesis, Aarhus University 2012
22. K.K. Andersen - Radiation emission from ultrarelativistic electrons, Ph.D. thesis, Aarhus University 2013

References

[1] K.K. Andersen *et al.*, Phys. Rev. Lett. **108**, 071802 (2012)
[2] R. Blankenbecler, Phys. Rev. D **55**, 190 (1997)
[3] V.N. Baier and V.M. Katkov, Phys. Rev. D **60**, 076001 (1999)
[4] R. Blankenbecler, Phys. Rev. D **55**, 2441 (1997)
[5] K.K. Andersen *et al.*, Phys. Rev. D, accepted for publ. (2013)
[6] K.K. Andersen, *et al.*, subm. to Phys. Rev. Lett. (2013)
[7] U.I. Uggerhøj on behalf of CERN NA63, CERN SPSC-2011-011; SPSC-P-327-ADD-2, Addendum to Proposal
[8] Allan H. Sørensen, "Electron-Ion Momentum Transfer at Ultrarelativistic Energy", in: Photonic, Electronic and Atomic Collisions; Invited Papers XX Int. Conf. on the Physics of Electronic and Atomic Collisions, eds. Friedrich Aumayr and Hannspeter Winter, (World Scientific, Singapore, 1998; ISBN 981-02-3425-2), 475-486.
[9] V.N. Baier, V.M. Katkov and V.M. Strakhovenko, *Electromagnetic Processes at High Energies in Oriented Single Crystals*, World Scientific 1998.
[10] J. Esberg *et al.*, Phys. Rev. D, **82**, 072002 (2010)
[11] K.K. Andersen *et al.*, Phys. Rev. D **86**, 072001 (2012)
[12] J.U. Andersen *et al.* (CERN NA63), CERN-SPSC-2005-030, SPSC-P-327 and CERN-SPSC-2005-016, SPSC-I-232
[13] U.I. Uggerhøj, Oral presentation to the SPSC, October 25th, 2011
[14] M.L. Ter-Mikaelian - High-Energy Electromagnetic Processes in Condensed Media, Wiley Interscience, 1972
[15] U.I. Uggerhøj, Rev. Mod. Phys. **77**, 1131 (2005)
[16] H.D. Thomsen, Ph.D. thesis, Aarhus University 2010
[17] J. Esberg, Ph.D. thesis, Aarhus University 2012
[18] K.K. Andersen, Ph.D. thesis, Aarhus University 2013
[19] H.D. Thomsen *et al.* (CERN NA63), Phys. Rev. D **81**, 052003 (2010)
[20] K.K. Andersen *et al.* (CERN NA63), CERN-SPSC-2009-038; SPSC-P-327-ADD-1, Addendum to Proposal
[21] P.L. Anthony *et al.*, Phys. Rev. D **56**, 1373 (1997)
[22] H.D. Hansen *et al.*, Phys. Rev. Lett. **91**, 014801 (2003)
[23] H.D. Hansen *et al.*, Phys. Rev. D **69**, 032001 (2004)
[24] S. Klein, Rev. Mod. Phys. **71**, 1501 (1999)
[25] A.B. Migdal, Phys. Rev. **103**, 1811 (1956)
[26] O. Dadoun *et al.*, Proceedings of IPAC'10, Kyoto, Japan; CLIC-Note-824
[27] X. Artru *et al.*, Phys Rev. ST-AB **6**, 091003 (2003)
[28] X. Artru *et al.*, Nucl. Instr. Meth. B **240**, 762 (2005)
[29] X. Artru *et al.*, Nucl. Instr. Meth. B **266**, 3868 (2008)
[30] V.N. Baier and V.M. Strakhovenko, Phys Rev. ST-AB **5**, 121001 (2002)
[31] T. Suwada *et al.*, Phys Rev. ST-AB **10**, 073501 (2007)
[32] M. Winter, Nucl. Instr. Meth. A **623**, 192 (2010)
[33] M. Satoh *et al.*, Nucl. Instr. Meth. B **227**, 3-10 (2005)